Supplementary Discussion

Alkanol Photooxidation Experiments. We injected pure organic seeds that do not dissolve in water using a custom-built evaporation-condensation generator modeled after Sinclair and La Mer [1], including DOS (97%, Sigma-Aldrich), oleic acid (99%, Fluka), and squalane (99% Sigma-Aldrich). For ammonium sulfate (99%, Fisher Chemical), sucrose (ACS grade, Fisher Chemical), and pentaethylene glycol (98% Sigma-Aldrich), injection was performed by atomizing (TSI 3076 Collison atomizer) and neutralizing (two TSI Model 3077) their water solution into the chamber. During the α-pinene/O_3-SOA-seeded experiments, we first injected 4-13 μL α-pinene (98%, Sigma-Aldrich) to the chamber through a glass bulb, which corresponds to ~45-140 ppb, followed by O_3 addition of ~110-200 ppb. The chamber was then left unperturbed for at least 1 h after which all α-pinene has reacted with O_3. After seed injection, we also measured seed wall loss for at least 30 min using SMPS. Then we injected 50 μL of 1-hexanol, 40 μL of 1-octanol, 25 μL of 1-nonanol, 18 μL of 1-decanol, and 12 μL of 1-dodecanol (all >99% purity, Sigma-Aldrich) into the chamber by gently heating the liquids (placed in a round-bottom glass vessel with gas ports) into a clean N_2 (UHP) flow. Finally, we injected 4 ppm of NO (99%, Matheson Trigas) and 4 ppm of methyl nitrite (MeONO, synthesized after the method of Taylor et al. [2]) into the chamber as pure gases using a small glass bulb and mixed the contents for 1 min before oxidation. One exception for the α-pinene/O_3 SOA experiments is that after ozonolysis has completed, we injected MeONO and NO first and turned on lights for 10 s. Thus we confirmed that there was no further SOA increase nor gaseous product that would interfere with our following SVOC measurements. Then we injected alkanols, followed by the normal fast oxidation. The OH exposure of the 10 s burst was determined by measuring the decays of butanediol or propanediol due to reaction with OH using an iodide CIMS. The average OH exposure for 9 repeated bursts using three different seeds (sucrose, squalane, and AS) and no seed is $4.4 \pm 0.3 \times 10^9$ molec cm^{-3} s. Prior to all experiments, the chamber bag was automatically filled to the same volume (using a differential pressure sensor for consistency) prior to seed injection and throughout a typical experiment, the bag volume decreased by ~6%.

Toluene Photooxidation Experiments. We also investigated the partitioning, in the presence of ammonium sulfate seeds, of products from toluene+OH oxidation under high NO (Table S1). The procedure is similar to the alkanol experiments, except that most oxidation bursts lasted for 20 s in order to produce measurable amounts of products, which corresponds to an OH exposure of $\sim 1.7 \times 10^{10}$ molecules cm^{-3} s. CIMS and AMS were used for two repeated experiments, respectively, with the same precursor concentrations. Fig. S9 shows the CIMS mass spectrum obtained shortly after the 20 s oxidation, containing products between *m/z* 200 – 600 (generally clustered with NO_3^-). Note that the background spectrum signals before oxidation are negligible except for reagent ions. We fitted the 260 most abundant high resolution (max. $m/\Delta m \sim 4000$) peaks and quantified the e-folding equilibrium time scales (τ) of the peaks that showed decay. Assuming the wall loss rate of these products is the same as alkanol products and their particle-phase wall loss is the same as the ammonium sulfate seeds, an $\sim 0.5 \leq \alpha \leq \sim 1$ would result in 200 s $< \tau \leq$ 300 s and $\sim 0.1 \leq \alpha < \sim 0.5$ corresponds to 300 s $< \tau <$ 500 s. The peaks that satisfy with these two ranges were labeled in Fig. S9. The presence of fast-condensing products indicates that important toluene condensing products do not have very low α ~ 0.001, contrary to what was previously reported [3].

In the particle phase, we did observe SOA formation ranging from 2 – 6 μg m^{-3} as the number of bursts increased, measured by both AMS (Fig. S10) and SMPS. Since the SOA-forming compounds are likely semivolatile, we assumed single c^* values for the measured bulk OA as the middle OA concentration half way through SOA formation immediately after each burst. Using

the assumed c^*, we modeled the AMS data similar to EESI-MS data and derived the optimum α values for the bulk SOA. The overall uncertainty in α was estimated by varying the chosen c^* up and down by a factor of 3, in addition to other uncertainties as included for CIMS and EESI-determined α. As shown in Fig. S11, α decreases from 0.6 to 0.3 as c^* increases from 2.8 to 16 μg m^{-3}, which is still much higher than 0.001. Using the direct, fast method, we observed evidence of relatively high α in both phases for some semivolatile products of toluene oxidation, which contradicts previous low α ~ 0.001.

Quantification of vapor wall loss. The wall loss of the oxidized compounds studied here was examined by conducting same oxidation reactions in the clean CU chamber without particles [4]. Once generated, the gas-phase concentration decrease can be attributed to gas-wall partitioning alone. The timescale (τ_W) for reaching equilibrium was determined by fitting the decay with an exponential curve. Thus we estimated $k_{G\rightarrow W}$ as $1/\tau_W$. C_w was calculated using initial and equilibrium gas-phase signals following the parameterization method in Krechmer et al. [4]. Averages for the 20 m^3 chamber from repeated experiments were shown in Fig. S2 as a function of c^*_{SIMPOL}. Previously, Krechmer et al. determined C_w for the same chemical system in an 8 m^3 Teflon chamber at 27 °C and dry conditions. After scaling C_w for the 8 m^3 chamber to the 20 m^3 chamber condition by temperature and surface-area-to-volume ratio, the C_w values for the same compounds for the two chambers agree reasonably (Fig. S2). We then performed a volatility-dependent parameterization of C_w using both sets of measurements and applied the parameterization to kinetic modeling. Note that for compounds with $c^*_{SIMPOL} < 10^{-1}$ μg m^{-3}, since they reside almost entirely in the walls at equilibrium and their relatively low CIMS S/N ratios can cause large uncertainties to C_w estimation, we used the same C_w parameterized at $c^*_{SIMPOL} = 10^{-1}$ μg m^{-3} for these relatively low volatility compounds. When there were seed particles, the choice of C_w for these low volatility compounds, either measured value or fixed value corresponding to $c^*_{SIMPOL} = 10^{-1}$ μg m^{-3}, would have negligible effect on model fitting as these compounds resided almost all in the particle phase.

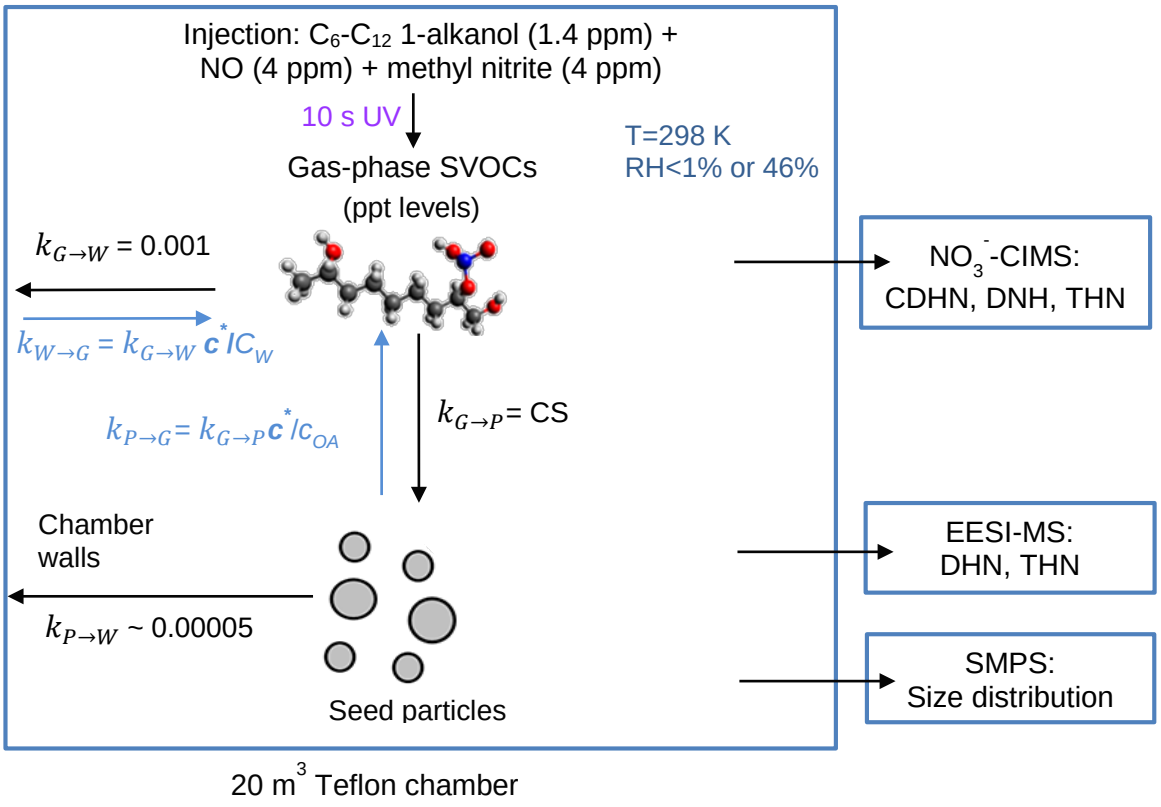

Supplementary Figure 1. Schematic of experimental procedures, instrumentation, and partitioning processes considered in this work. All rate constants are in units of s^{-1}. Note that the dependence of the system on α is embedded in the condensational sink term (CS) within the Fuchs-Sutugin correction.

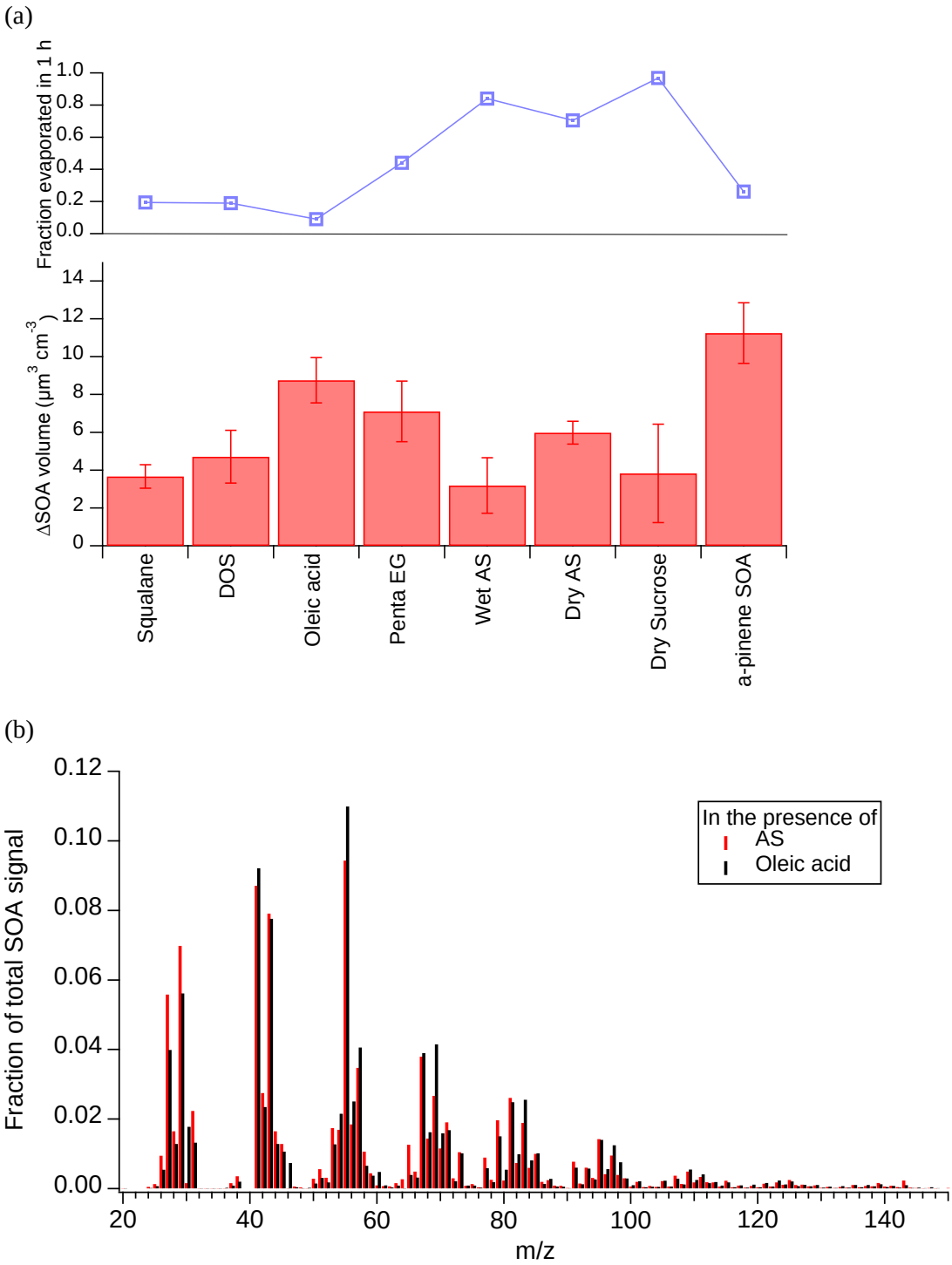

Supplementary Figure 2. (a) Peak SOA volume produced immediately after the OH oxidation burst, and the fraction evaporated after 1 h for the different seeds used in this study. Error bars are standard deviations across all experiments with a given seed (including experiments with different *CS*). (b) Example of SOA mass spectrum of an AS- and an oleic-acid-seeded experiment as measured by an aerosol mass spectrometer (AMS) [5]. The seed spectrum has been subtracted.

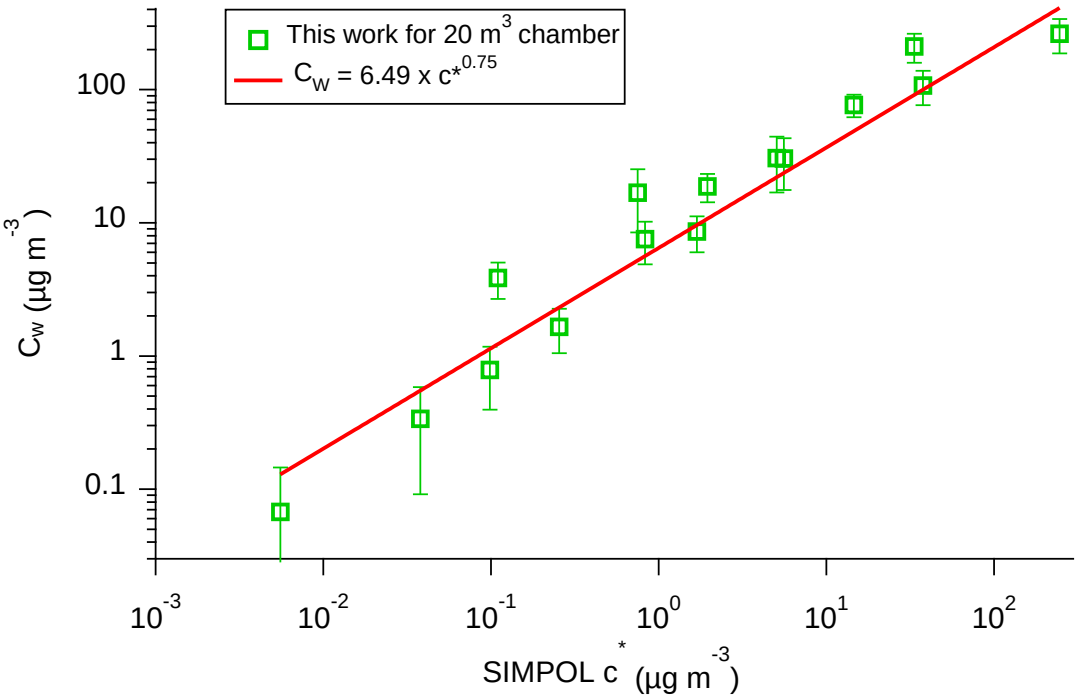

Supplementary Figure 3. Average equivalent wall mass concentration (C_W) as a function of SIMPOL c^* for measured species in this work. Error bars represent standard deviations. The red line shows the functions that parameterize this dependence on the SIMPOL c^*.

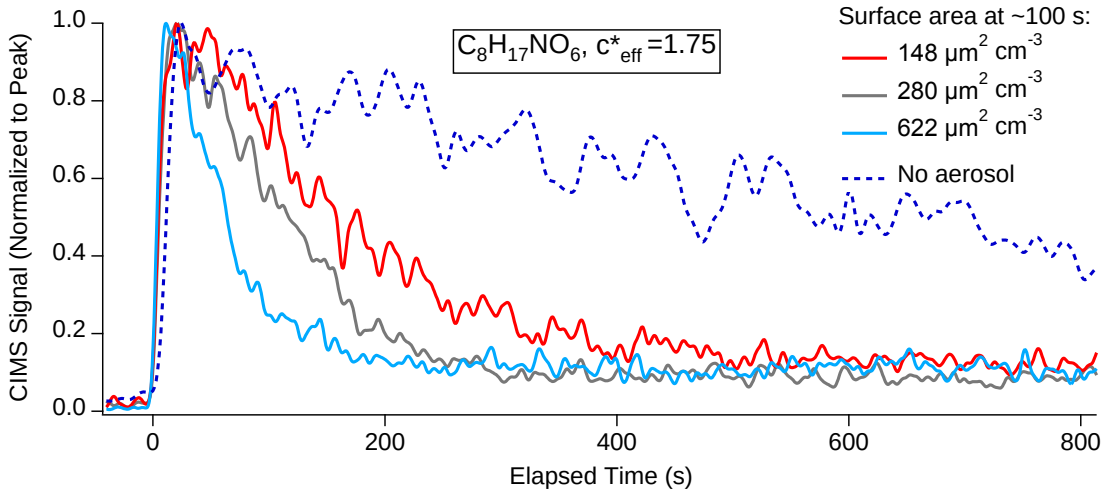

Supplementary Figure 4. NO_3-CIMS time evolution of $C_8H_{17}NO_6$ THNs in the presence of oleic acid seed aerosol with varying concentrations. Surface area and size distributions are dynamic, and so is condensation rate. A legend lists surface areas at ~100 s after oxidation. This THN condenses at increasing rates with higher aerosol surface areas. All traces have been binomially smoothed across 20 points for visual clarity and normalized to the maximum for comparison. Note that between 600-800 s when a steady state is reached, the fraction in the gas phase should be ~10% for all the seeded cases according to partitioning theory (given model fitted $\boldsymbol{C^*_{eff}}$), thus detected as similar gas-phase CIMS signals.

(a)

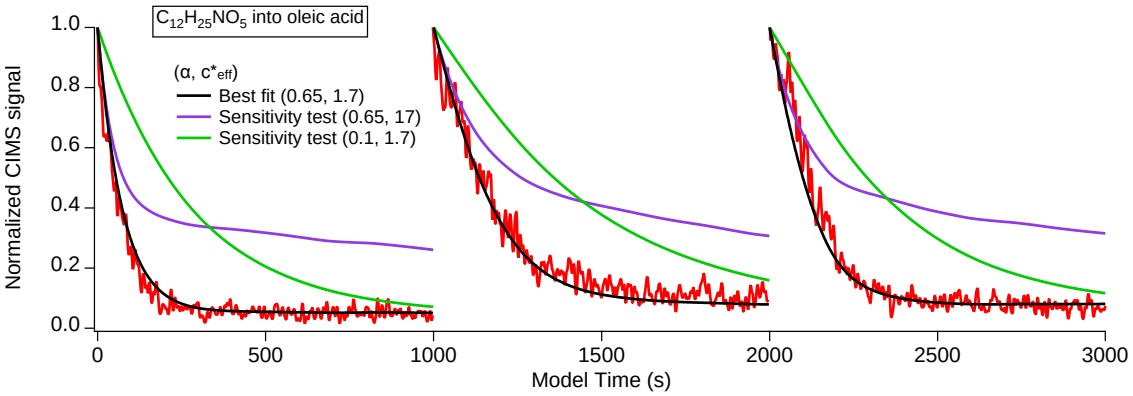

(b)

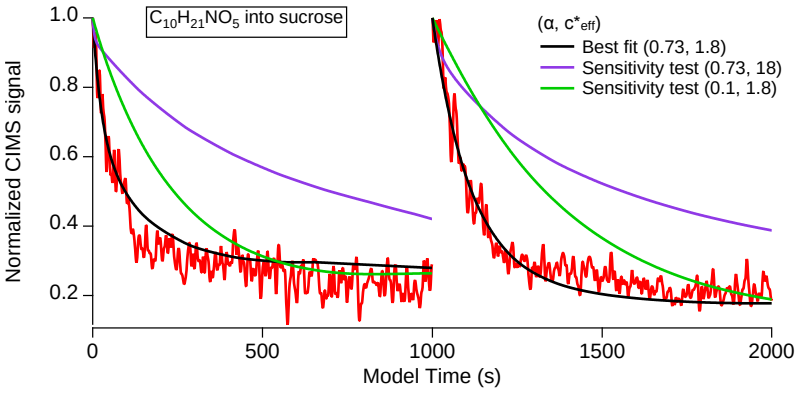

(c)

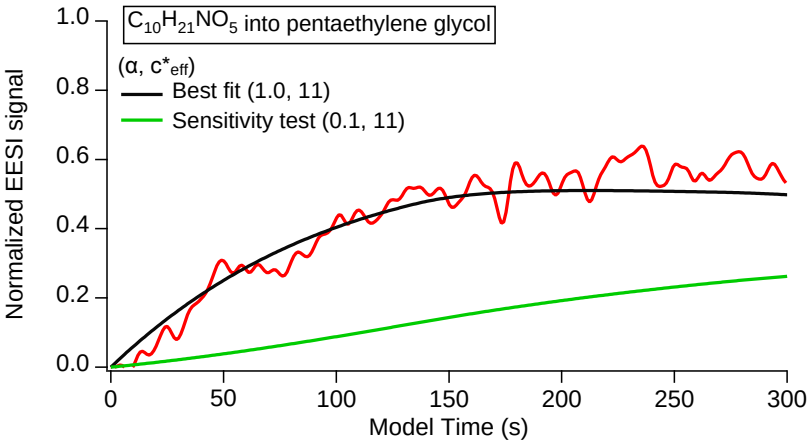

Supplementary Figure 5. Example measurement traces, best model fits, and several model traces with alternative α and *c** parameters for (a) NO_3-CIMS measured $C_{12}H_{25}NO_5$ during three oleic acid seed experiments, (b) NO_3-CIMS measured $C_{10}H_{21}NO_5$ during two dry sucrose seed experiments, and (c) EESI-MS measured $C_{10}H_{21}NO_5$ during a pentaethylene glycol seed experiment. Each decay measurement shown was obtained in separate experiments, while the time axis increases only for the purpose of model fitting. Measurement traces were binomially smoothed across 10 points to reduce high-frequency noise. All traces normalized to initial gas phase maximum concentrations.

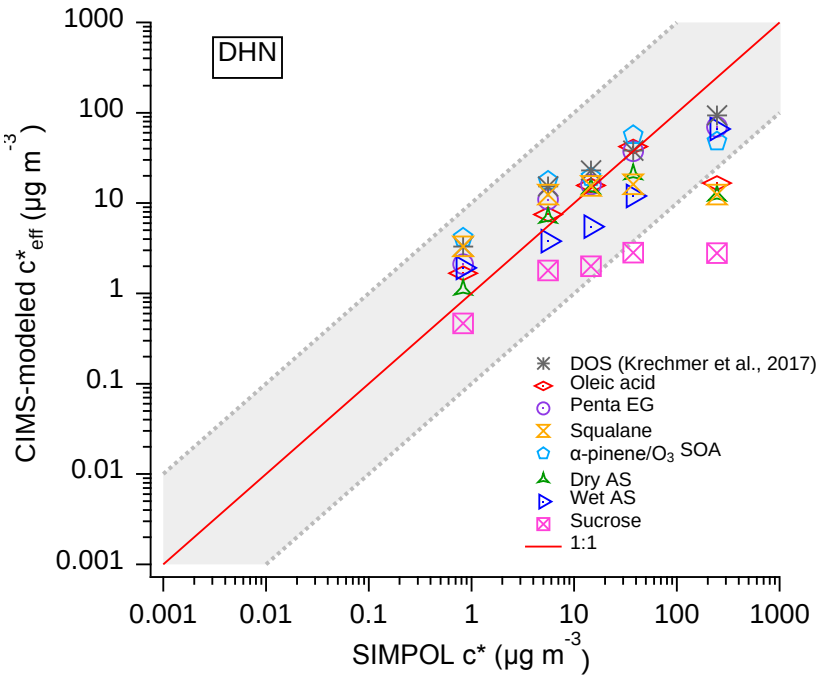
DHN
CIMS-modeled c*eff (μg m-3)
SIMPOL c* (μg m-3)
1000
100
10
1
0.1
0.01
0.001
0.001
0.01
0.1
1
10
100
1000
DOS (Krechmer et al., 2017)
Oleic acid
Penta EG
Squalane
α-pinene/O3 SOA
Dry AS
Wet AS
Sucrose
1:1

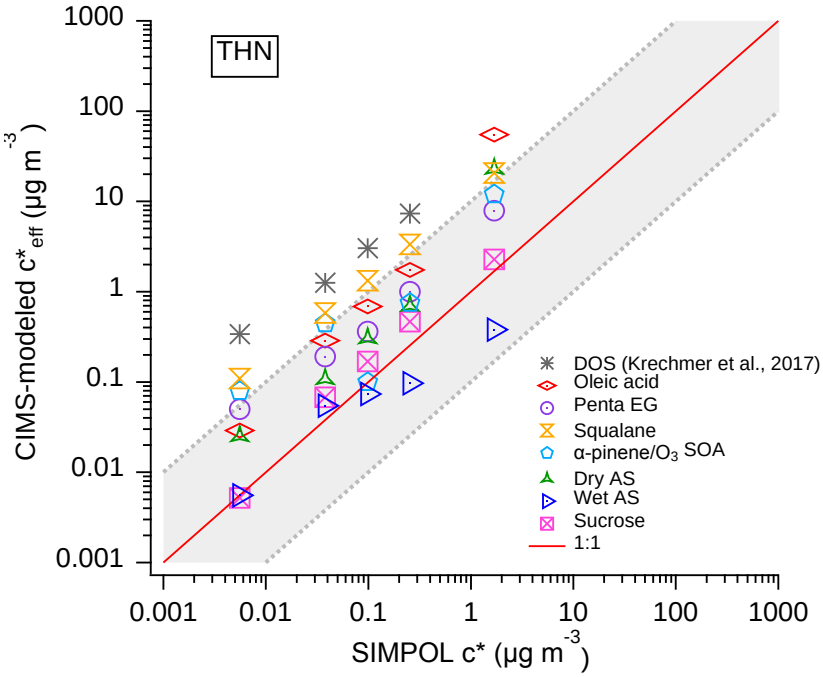
THN
CIMS-modeled c*eff (μg m-3)
SIMPOL c* (μg m-3)
1000
100
10
1
0.1
0.01
0.001
0.001
0.01
0.1
1
10
100
1000
DOS (Krechmer et al., 2017)
Oleic acid
Penta EG
Squalane
α-pinene/O3 SOA
Dry AS
Wet AS
Sucrose
1:1

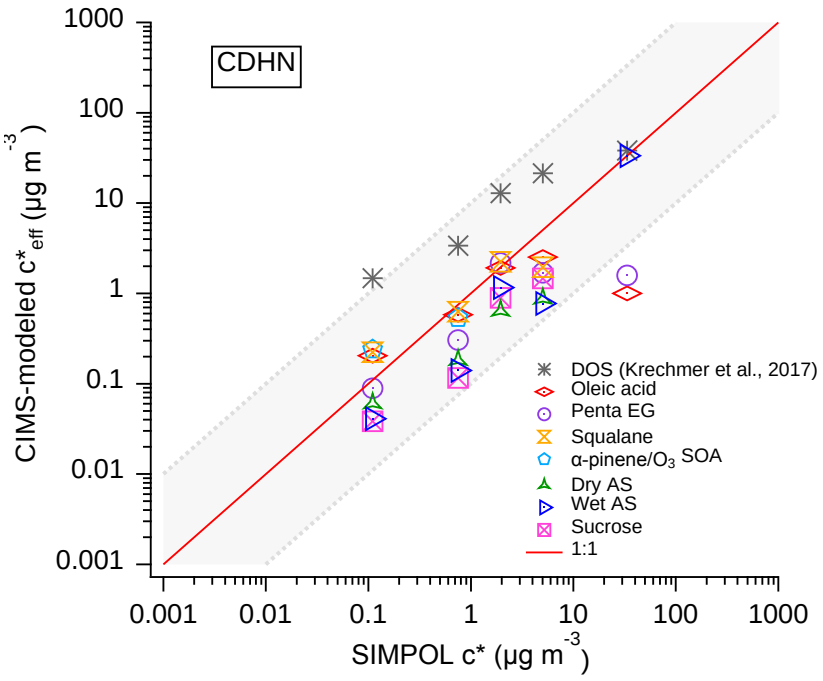

Supplementary Figure 6. Effective saturation concentrations (c^*_{eff}, determined from fitting of CIMS measurements) as a function of SIMPOL-estimated c* values for the compounds in this study. c^*_{eff} for DOS was adopted from Krechmer et al. [6] and adjusted by multiplying $\frac{MW_i}{MW}$ so to be consistent with c^*_{eff} for other seeds derived in this study (see equations [5-6]). The gray area represents the estimated uncertainty of SIMPOL of +/- 1 order of magnitude. c^*_{eff} values for same compounds differ for different seeds, likely contributed by variability in activity coefficient γ.

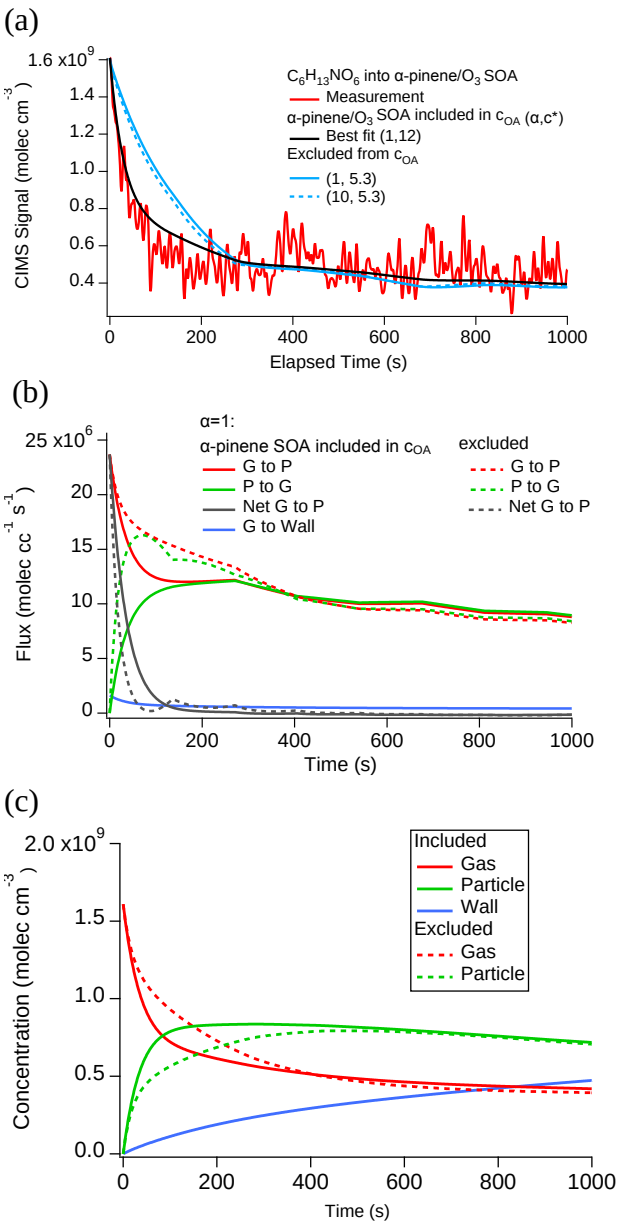

Supplementary Figure 7. Examples of modeling $C_6H_{13}NO_6$ THNs partitioning into α-pinene/O_3 SOA by including and excluding the SOA in the partitioning c_{OA} with α =1. (a) Comparison of modeled gas-phase decay for two scenarios. Note that excluding α-pinene/O_3 SOA from c_{OA} cannot yield realistic α. This is also shown in Fig. 4. (b) Comparison of phase partitioning rates. (c) Comparison of phase concentrations, where SMPS measurements were smoothed across 3 points to generate a smooth evolution as an illustration. The initial concentration is assumed to be 1.6×10^9 molec cm^{-3}.

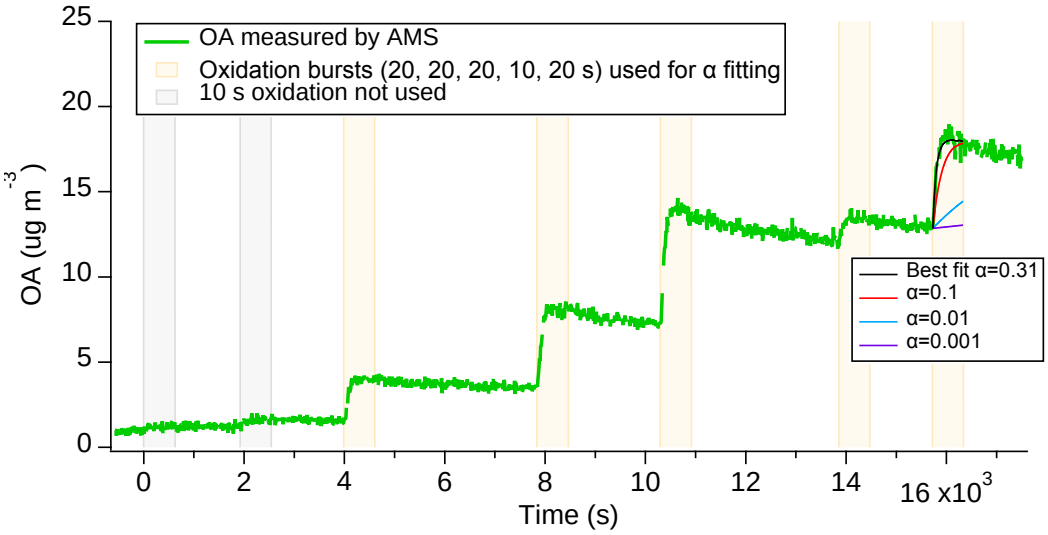

Supplementary Figure 8. OA time series during a toluene/OH experiment as measured by AMS with time resolution ~ 10 s. Oxidation bursts used for α calculation are labeled. The first two bursts were not used due to low amounts of SOA generated. The bursts lasted for 10-20 s while the shaded areas (600 s) are time periods used for modeling. Also shown are fitting examples for the last burst, including best model fits, and several model traces with smaller α.

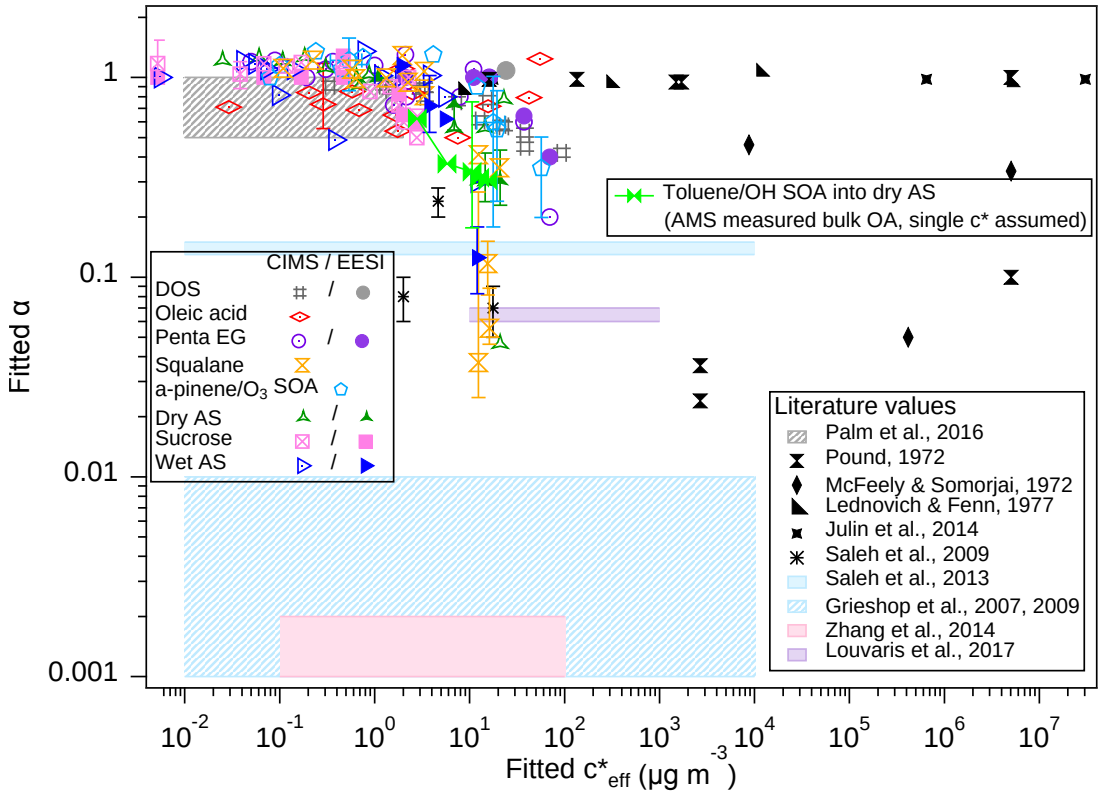

Supplementary Figure 9. Mass accommodation coefficients (α) determined from AMS measurements of toluene/OH experiments added to Fig. 3. See Fig. 3 for details of other data points.

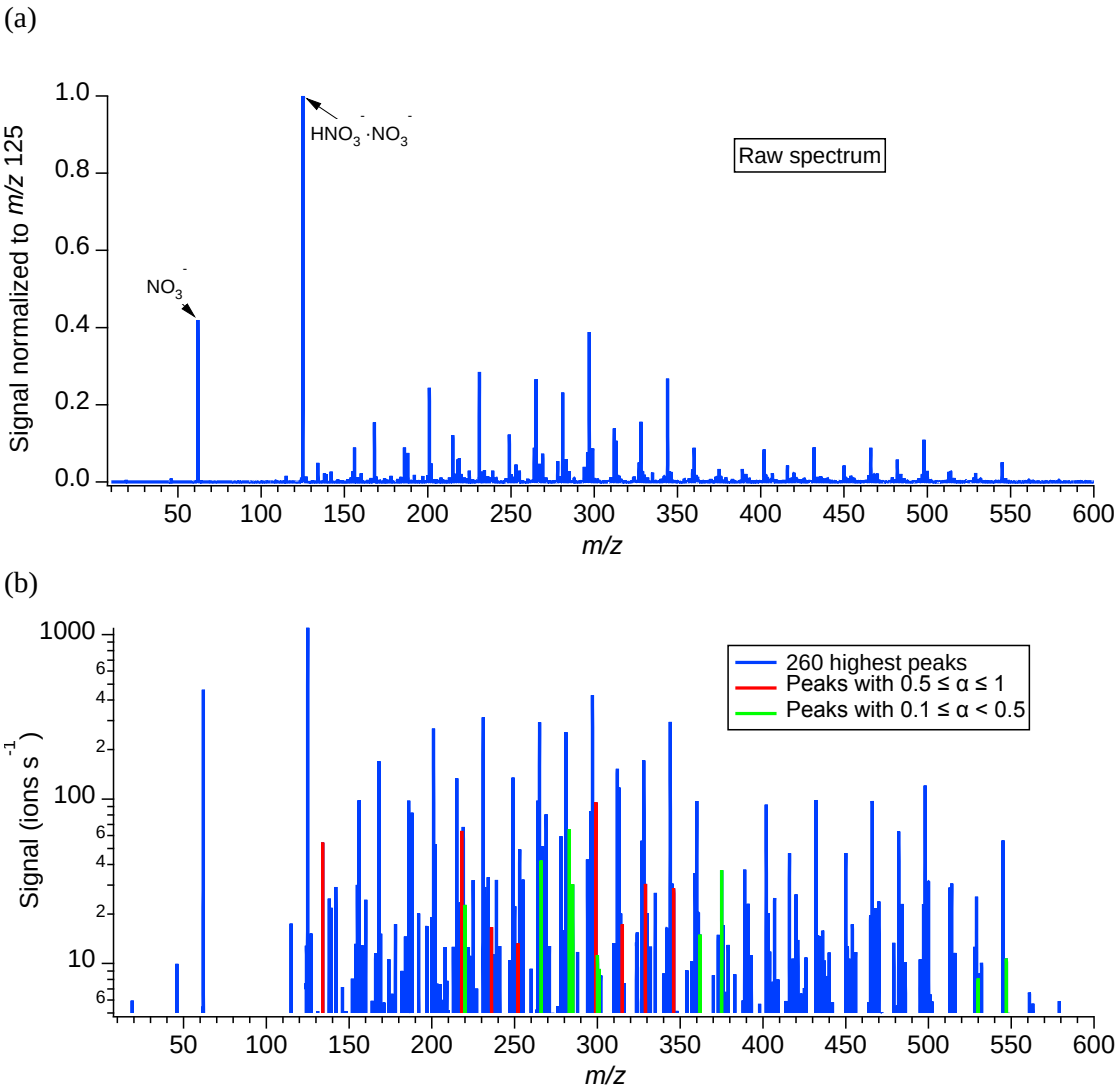

Supplementary Figure 10. NO_3-CIMS mass spectrum shortly after 20 s OH oxidation of toluene under high NO_x. (a) Raw mass spectrum with signals normalized to one of the reagent ions, *m/z* 125 ($HNO_3 \cdot NO_3^-$). Note that the background signals before oxidation are negligible except for reagent ions. (b) Among the 260 most abundant high-resolution peaks, peaks that show decay time scales (τ) corresponding to ~0.1 ≤ α < ~0.5 (300 s < τ < 500 s) and ~0.5 ≤ α ≤ ~1 (200 s < τ ≤ 300 s) are highlighted.

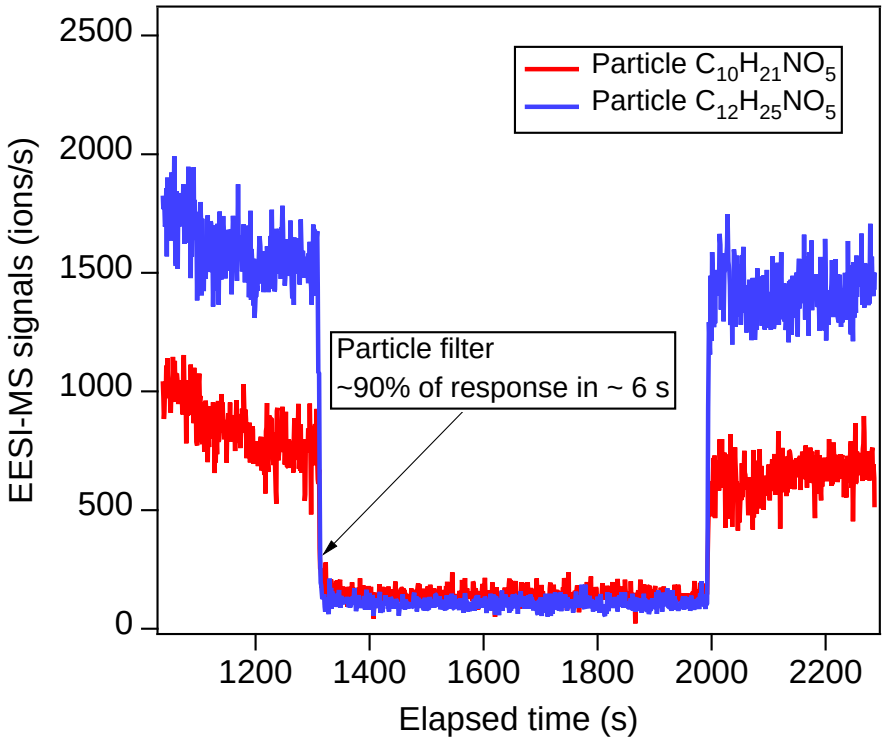

Supplementary Figure 11. Example of EESI-MS signals of two DHNs before, during, and after passing through an aerosol filter. The rapid (~6 s) EESI-MS response to changes in concentration warrants its applicability in measuring fast partitioning processes.

Supplementary Table 1. The alkanol oxidation products measured in this study. Products are grouped by compound and classified as the following: CDHN=dihydroxycarbonylnitrate, DHN=dihydroxynitrate, THN=trihydroxynitrate, and HN=hydroxynitrate. CIMS measures all three classes of compounds, while EESI-MS measures DHNs and THNs. Note that these MS techniques cannot distinguish structural isomers of these species.

Compound Class	Formula	MW	Precursor	SIMPOL c^* (μg m^{-3})
CDHN	$C_6H_{11}NO_6$	193.155	Hexanol	3.34E+01
CDHN	$C_8H_{15}NO_6$	221.208	Octanol	5.05E+00
CDHN	$C_9H_{17}NO_6$	235.234	Nonanol	1.95E+00
CDHN	$C_{10}H_{19}NO_6$	249.261	Decanol	7.50E-01
CDHN	$C_{12}H_{23}NO_6$	277.314	Dodecanol	1.10E-01
DHN	$C_6H_{13}NO_5$	179.171	Hexanol	2.46E+02
DHN	$C_8H_{17}NO_5$	207.224	Octanol	3.76E+01
DHN	$C_9H_{19}NO_5$	221.251	Nonanol	1.46E+01
DHN	$C_{10}H_{21}NO_5$	235.277	Decanol	5.57E+00
DHN	$C_{12}H_{25}NO_5$	263.331	Dodecanol	8.29E-01
THN	$C_6H_{13}NO_6$	195.171	Hexanol	1.69E+00
THN	$C_8H_{17}NO_6$	223.224	Octanol	2.55E-01
THN	$C_9H_{19}NO_6$	237.250	Nonanol	9.85E-02
THN	$C_{10}H_{21}NO_6$	251.277	Decanol	3.79E-02
THN	$C_{12}H_{25}NO_6$	279.330	Dodecanol	5.55E-03

Supplementary Table 2. Summary of chamber experiments used in this study.

Alkanol oxidation								
Seed	No.	RH (%)	CIMS/EESI-MS	1-alkanol precursor	Total Alkanol conc. (ppm)	Start seed S.A. (μm^2 cm^{-3})	Start seed conc. (μg m^{-3})	k_{cs} (10^{-3} s^{-1}) (with $\alpha = 1$)
Oleic acid	1	<1	CIMS	C6,8,9,10,12	1.4	494	15.6	14
	2	<1	CIMS	C6,8,9,10,12	1.4	120	2.91	3.8
	3	<1	CIMS	C6,8,9,10,12	1.4	69	1.75	2.1
Squalane	1	<1	CIMS	C6,8,9,10,12	1.4	1118	26.6	34
	2	<1	CIMS	C6,8,9,10,12	1.4	458	10.8	14
Pentaethylene glycol	1	<1	CIMS	C6,8,9,10,12	1.4	231	3.95	8.2
	2	<1	CIMS	C6,8,9,10,12	1.4	473	7.85	16
	3	<1	EESI-MS	C6,8,9,10,12	1.4	171	4.51	5.5
α-pinene/O_3 SOA	1	<1	CIMS	C6,8,9,10,12	1.4	2492	107	71
	2	<1	CIMS	C6,8,9,10,12	1.4	464	15.0	15
Ammonium sulfate	1	<1	CIMS	C6,8,9,10	0.7	998	44.3	35
	2	<1	CIMS	C6,8,9,10,12	1.4	158	6.20	5.2
	3	<1	CIMS	C8,10,12	0.6	501	18.6	17
	4	<1	EESI-MS	C6,8,9,10,12	1.4	182	9.44	5.4
	5	46	CIMS	C6,8,9,10,12	1.4	182	12.5	4.9
	6	45	CIMS	C6,8,9,10,12	1.4	540	30.2	14
	7	46	EESI-MS	C6,8,9,10,12	1.4	444	14.1	14
Sucrose	1	<1	CIMS	C6,8,9,10,12	1.4	566	32.1	16
	2	<1	CIMS	C6,8,9,10,12	1.4	200	10.4	5.8
	3	<1	EESI-MS	C6,8,9,10,12	1.4	436	21.6	13
DOS	1	<1	EESI-MS	C10	0.09	416	11.4	12

Toluene oxidation								
Seed	No.	RH (%)	CIMS/AMS	Toluene conc. (ppm)	NO conc. (ppm)	Start seed S.A. (μm^2 cm^{-3})	Start seed conc. (μg m^{-3})	k_{cs} (10^{-3} s^{-1}) (with $\alpha = 1$)
Ammonium sulfate	1	<1	CIMS	0.78	0.98	168	9.01	4.9
	2	<1	AMS	0.78	0.99	605	26.4	18

Supplementary Table 3. Correlation of SOA UMR spectra measured by AMS in the presence of different seeds, with AS seed experiment as a reference. High correlations were observed for SOA generated in different experiments. As a comparison, seed particles, e.g., sucrose and squalane, correlate much less well with SOA.

	Pearson R	**Uncentered R**
SOA with AS	-	-
SOA with sucrose	0.959	0.962
SOA with squalane	0.921	0.926
SOA with oleic acid	0.976	0.978
Sucrose	0.679	0.702
Squalane	0.563	0.578

Supplementary References

1. Sinclair D., La Mer V. K. Light Scattering as a Measure of Particle Size in Aerosols. The Production of Monodisperse Aerosols. *Chem. Rev.* **44**, 245-267 (1949).

2. Taylor W. D., Allston T. D., Moscato M. J., Fazekas G. B., Kozlowski R., Takacs G. A. Atmospheric photodissociation lifetimes for nitromethane, methyl nitrite, and methyl nitrate. *Int. J. Chem. Kinet.* **12**, 231-240 (1980).

3. Zhang X., *et al.* Influence of vapor wall loss in laboratory chambers on yields of secondary organic aerosol. *Proc. Natl. Acad. Sci. USA* **111**, 5802-5807 (2014).

4. Krechmer J. E., Pagonis D., Ziemann P. J., Jimenez J. L. Quantification of Gas-Wall Partitioning in Teflon Environmental Chambers Using Rapid Bursts of Low-Volatility Oxidized Species Generated in Situ. *Environ. Sci. Technol.* **50**, 5757-5765 (2016).

5. DeCarlo P. F., *et al.* Field-Deployable, High-Resolution, Time-of-Flight Aerosol Mass Spectrometer. *Anal. Chem.* **78**, 8281-8289 (2006).

6. Krechmer J. E., Day D. A., Ziemann P. J., Jimenez J. L. Direct Measurements of Gas/Particle Partitioning and Mass Accommodation Coefficients in Environmental Chambers. *Environ. Sci. Technol.* **51**, 11867-11875 (2017).